

Magneto-electric equivalence and emergent electrodynamics in bilayer graphene

R. Winkler^{1,2,3,4} and U. Zülicke⁵

¹*Department of Physics, Northern Illinois University, DeKalb, Illinois 60115, USA*

²*Materials Science Division, Argonne National Laboratory, Argonne, Illinois 60439, USA*

³*Department of Physical Chemistry, The University of the Basque Country, 48080 Bilbao, Spain*

⁴*IKERBASQUE, Basque Foundation for Science, 48011 Bilbao, Spain*

⁵*School of Chemical and Physical Sciences and MacDiarmid Institute for Advanced Materials and Nanotechnology, Victoria University of Wellington, PO Box 600, Wellington 6140, New Zealand*

(Dated: Version of February 26, 2024. Not for distribution!)

It is a fundamental paradigm that the physical effects induced by electric fields are qualitatively different from those induced by magnetic fields. Here we show that electrons at a Dirac point in bilayer graphene experience an unusual type of electromagnetism where magnetic and electric fields are virtually equivalent: every coupling of an electron's degrees of freedom to a *magnetic* field is matched by an analogous coupling of the *same* degrees of freedom to an *electric* field. This counter-intuitive duality of matter-field interactions enables novel ways to create and manipulate spin and pseudo-spin polarizations in bilayer graphene via external fields and leads to the emergence of a valley-contrasting axion electrodynamics, where the traditional association of charges at rest with electric fields and charge currents with magnetic fields is reversed.

I. INTRODUCTION

The dynamics of charge carriers in crystalline solids normally resembles that exhibited by free electrons, only with numerical values of parameters such as mass and gyromagnetic ratio renormalized due to the influence of the crystal structure.¹ In certain instances, changes in the properties of band electrons turn out to be dramatic. Few-layer samples of graphite^{2,3} are one example, and a new class of so-called *topological* materials⁴ another. Here we focus on bilayer graphene^{5,6} (BLG), i.e., two single-layer sheets of graphite stacked as shown in Fig. 1(a). Electrons in this material turn out to be pseudospin-carrying chiral fermions having a finite band mass but zero rest energy.⁷ Our study shows that the interaction of these exotic charge carriers with electromagnetic fields is very unusual. Normally, electric fields couple to electric charges at rest and moving magnetic moments, whereas magnetic fields couple to moving electric charges and magnetic moments at rest. In contrast, every coupling of a bilayer electron's degree of freedom to an electric field is matched by an analogous coupling to a magnetic field. We explore physical consequences of this magneto-electric equivalence, including anomalous polarizations of real spin and the layer-index-related pseudospin, as well as an anisotropic version of axion electrodynamics.⁸

The BLG band structure near the \mathbf{K} point in the Brillouin zone [see Fig. 1(b)] is described by the effective Hamiltonian

$$\mathcal{H}_{\mathbf{K}}(\mathbf{k}) = -\frac{\hbar^2}{2m_1} (k_+^2 \sigma_+ + k_-^2 \sigma_-) + \frac{\hbar^2 k^2}{2m_2} \sigma_0 - \hbar v_3 (k_- \sigma_+ + k_+ \sigma_-), \quad (1)$$

where \hbar is Planck's constant, $\mathbf{k} \equiv (k_x, k_y)$ is the electrons' wave vector measured from \mathbf{K} , and the Pauli matrices $\sigma_{x,y,z}$ are associated with the sublattice (or, equivalently,

the layer-index) pseudospin degree of freedom.³ In our notation, σ_0 is the 2×2 unit matrix, $\sigma_{\pm} = (\sigma_x \pm i\sigma_y)/2$, and $k_{\pm} = k_x \pm ik_y$. Numerical values for the effective masses m_j and the speed v_3 are well known.^{3,6} Very close to the \mathbf{K} point, the energy dispersion resulting from (1) mimics that of massless Dirac electrons, as is the case in single-layer graphene (SLG). However, as $m_1 \ll m_2$, the dominant behavior of electrons in BLG is captured by the quadratic dispersion shown in Fig. 1(c).

External fields can have striking effects on the electronic properties of charge carriers in solids. Previously, only the effects of electric fields \mathcal{E}_z and magnetic fields B_z directed perpendicular to the BLG sheet have been

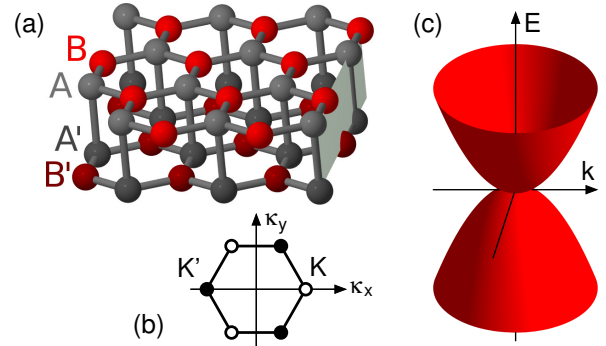


FIG. 1: Basic structural and electronic properties of bilayer graphene. (a) Honeycomb structure of a bilayer stack of graphene. Atoms in sublattice A (B) are marked in grey (red). A yz plane is marked in light grey. (b) Brillouin zone and its two inequivalent corner points \mathbf{K} and \mathbf{K}' . The remaining corners are related with \mathbf{K} or \mathbf{K}' by reciprocal lattice vectors. (c) Dispersion $E(k)$ near the \mathbf{K} point. We have $\mathbf{k} \equiv \boldsymbol{\kappa} - \mathbf{K}$.

TABLE I: Magneto-electric equivalence of matter-field interactions in BLG. In each row, the coupling of an electron's degrees of freedom to a magnetic field \mathbf{B} (left) is matched by an analogous coupling to an electric field \mathcal{E} (right). In these pairs, \mathbf{B} and \mathcal{E} couple identically to the real spin \mathbf{s} and pseudospin $\boldsymbol{\sigma}$, while the coupling to the valley isospin $\boldsymbol{\tau}$ is opposite: For one field, the coupling has the same sign in both valleys (isospin τ_0), for the other field it has opposite signs (isospin τ_z). In each row, the interaction unique to BLG is marked by \star , while the other one exists also in SLG.⁹ The interactions are visualized in Fig. 2.

magnetic field \mathbf{B}		electric field \mathcal{E}	
orbital Zeeman splitting (\perp field)	$B_z \sigma_z \tau_z$ (1)	$\mathcal{E}_z \sigma_z \tau_0$	inter-layer (pseudo-spin) gap \star
magnetic spin splitting (\perp field)	$B_z s_z \tau_0$ (2)	$\mathcal{E}_z s_z \tau_z$	electric spin splitting (\perp field) \star
magnetic spin splitting (\parallel field)	$(B_x s_x + B_y s_y) \tau_0$ (3)	$(\mathcal{E}_x s_x + \mathcal{E}_y s_y) \tau_z$	electric spin splitting (\parallel field) \star
spin-orbital Zeeman (\perp field) \star	$B_z (s_y \sigma_x \tau_0 - s_x \sigma_y \tau_z)$ (4)	$\mathcal{E}_z (s_y \sigma_x \tau_z - s_x \sigma_y \tau_0)$	Rashba spin splitting (\perp field)
spin-orbital Zeeman (\parallel field) \star	$s_z (B_y \sigma_x \tau_0 - B_x \sigma_y \tau_z)$ (5)	$s_z (\mathcal{E}_y \sigma_x \tau_z - \mathcal{E}_x \sigma_y \tau_0)$	Rashba spin splitting (\parallel field)
orbital Zeeman splitting (\parallel field) \star	$(k_x B_y - k_y B_x) \sigma_z \tau_0$ (6)	$(k_x \mathcal{E}_y - k_y \mathcal{E}_x) \sigma_z \tau_z$	orbital Rashba splitting
trigonal Zeeman splitting	$(s_y B_y - s_x B_x) \sigma_x \tau_0$ (7)	$(s_y \mathcal{E}_y - s_x \mathcal{E}_x) \sigma_x \tau_z$	trigonal Rashba splitting \star
	$+(s_x B_y + s_y B_x) \sigma_y \tau_z$	$+(s_x \mathcal{E}_y + s_y \mathcal{E}_x) \sigma_y \tau_0$	

considered, giving the extended effective Hamiltonian

$$\mathcal{H}_{\mathbf{K}}(\mathbf{k}, \mathcal{E}_z, B_z) = \mathcal{H}_{\mathbf{K}}(\mathbf{k} + e\mathbf{A}) + \frac{\lambda_z}{2} \mathcal{E}_z \sigma_z - \frac{g}{2} \mu_B B_z \sigma_z + c_z \mathcal{E}_z B_z \sigma_0. \quad (2)$$

Accordingly, (i) a potential difference between the two layers (equivalent to finite \mathcal{E}_z) opens up a pseudospin gap^{6,10} $\lambda_z \mathcal{E}_z$, (ii) B_z induces a pseudospin Zeeman splitting¹¹ $g \mu_B B_z$, and (iii) the simultaneous presence of fields \mathcal{E}_z and B_z leads to an (actually, valley-contrasting – see below) overall energy shift^{11–13} $c_z \mathcal{E}_z B_z$. In Eq. (2), g is the gyromagnetic ratio, μ_B is the Bohr magneton, and \mathbf{A} is the electromagnetic vector potential satisfying $(\nabla \times \mathbf{A})_z = B_z$. The matter-field interactions (i)–(iii) generate sizeable effects for typical values of \mathcal{E}_z and B_z (see Appendix C). In addition, the chiral nature of electrons in BLG leads to unconventional quantum-Hall physics.^{5,6}

II. MAGNETO-ELECTRIC EQUIVALENCE IN BLG: ORIGIN & PHYSICAL CONSEQUENCES

Inspection of Eq. (2) reveals a surprising feature: disregarding constant prefactors, the electron's interaction with fields \mathcal{E}_z and B_z is symmetric with respect to the interchange of \mathcal{E}_z and B_z . Indeed, this observation is not an accident. It reflects the unusual property of BLG that its crystal symmetry does not distinguish between polar vectors such as the electric field \mathcal{E} and axial vectors such as the magnetic field \mathbf{B} . Moreover, the familiar constraints due to time-reversal invariance are modified in BLG such that symmetry under time reversal likewise permits that \mathcal{E} and \mathbf{B} become interchangeable.

Using symmetry^{9,14,15} we have obtained the complete set of interactions of electrons near the \mathbf{K} point in BLG with magnetic and electric fields \mathbf{B} and \mathcal{E} , strain $\boldsymbol{\epsilon}$, and also spin \mathbf{s} . See Appendix A for details on our method and full results. All interactions that exist in SLG are also present in BLG. In addition, there are new interactions in BLG that can be obtained from field-dependent

SLG interactions by replacing the magnetic (electric) field components with their electric (magnetic) counterparts. Table I summarizes this magneto-electric equivalence for couplings that are linear in electric or magnetic field components. The interaction $\propto \mathcal{E}_z \sigma_z$ coupling the pseudospin to a perpendicular electric field thus arises by magneto-electric equivalence from the pseudospin Zeeman term $\propto B_z \sigma_z$ that exists in SLG. Moreover, we obtain a rather counter-intuitive purely electric-field-dependent spin splitting $\propto \mathcal{E}_z s_z$, which can be directly measured using electron spin resonance. Also interesting is the spin-orbital Zeeman splitting $\propto B_z (s_y \sigma_x - s_x \sigma_y)$, which is the magneto-electric equivalent of Rashba spin splitting in SLG.¹⁶ We note that the electrons interact not only with the fields \mathbf{B} and \mathcal{E} , but their quantum dynamics depends also – via the usual minimal coupling¹ – on the electromagnetic potentials \mathbf{A} and Φ . The latter contributions are not affected by the magneto-electric equivalence.

A. Spin textures

The interactions shown in Table I give rise to a diverse set of textures for the induced spin and pseudospin orientations in \mathbf{k} space, which are illustrated in Fig. 2. The grey arrow in the lower left of each panel indicates the direction of the external field while a large arrow in the lower right indicates (if present) the spin polarization induced by the particular interaction when averaging over all occupied states in the $k_x k_y$ plane.

In addition to the layer-index pseudospin $\boldsymbol{\sigma}$, electrons in BLG carry a valley-isospin $\boldsymbol{\tau}$ that distinguishes states near the two inequivalent \mathbf{K} and $\mathbf{K}' \equiv -\mathbf{K}$ points in the Brillouin zone³ [Fig. 1(b)]. The effective Hamiltonian for electrons in the \mathbf{K}' valley can be obtained from that for the \mathbf{K} valley by a reflection of the vectors \mathbf{k} , \mathbf{s} , \mathcal{E} , and \mathbf{B} at the yz plane, see Fig. 1(a).⁹ Choosing the convention that the \mathbf{B} and \mathcal{E} -dependent terms have the same sign in the \mathbf{K} valley (first column of Fig. 2), the corre-

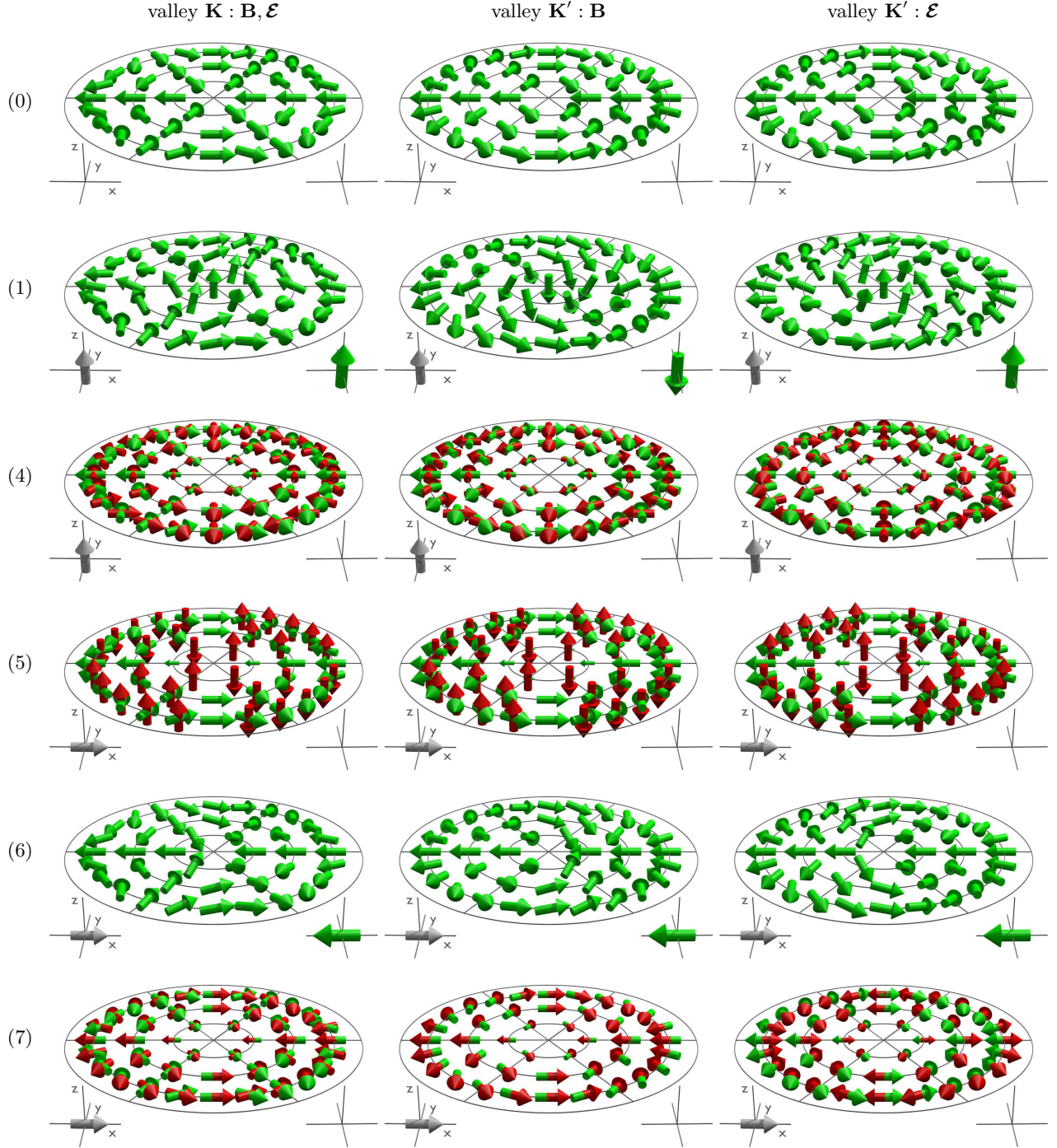


FIG. 2: Visualization of real and pseudo-spin textures in BLG generated by field-dependent interactions shown in Table I [omitting the trivial interactions (2) and (3)]. For selected points in \mathbf{k} space, a red (green) arrow indicates the expectation value of the real (pseudo-)spin vector of the corresponding negative-energy eigenstate obtained by diagonalizing the leading field-independent contribution to the BLG Hamiltonian together with the interaction associated with the same number in Table I. The 1st (2nd, 3rd) column shows results for the \mathbf{K} (\mathbf{K}' with \mathbf{B} , \mathbf{K}' with \mathbf{E}) valley. Note that our sign convention is such that \mathbf{B} and \mathbf{E} have the same effect in the \mathbf{K} valley (1st column). Grey arrows indicate the direction of the applied field. The first row denoted (0) shows the pseudo-spin orientation without any external fields. Big arrows in the lower right of the panels indicate the existence of a net spin polarization obtained by averaging over the (pseudo-)spin expectation values of occupied hole states for a negative chemical potential.

sponding term in the \mathbf{K}' valley involving the axial vector \mathbf{B} (second column) differs by an overall minus sign from the term involving the polar vector \mathcal{E} (third column of Fig. 2, see also Table I). For example, the orbital Zeeman term $\propto B_z \sigma_z \tau_z$ couples B_z to the pseudospin associated with the sublattice degree of freedom σ_z . However, the field B_z does not induce a global pseudo-spin (sublattice) polarization, because this term has opposite signs in the two valleys so that the pseudospin polarization in the two valleys is antiparallel. As a result, the two sublattices remain indistinguishable even for finite B_z . Only an electric field \mathcal{E}_z polarizes the sublattices in BLG via the term $\propto \mathcal{E}_z \sigma_z \tau_0$, consistent with the fact that the pseudospin σ_z is even under time reversal.¹⁷ This behaviour is opposite to that of real spin, where $B_z s_z \tau_0$ induces a real-spin polarization $\langle s_z \rangle$ (when averaging over the occupied states in both valleys) while the term $\mathcal{E}_z s_z \tau_z$ does not, consistent with time reversal symmetry. Similarly, an in-plane magnetic field \mathbf{B}_{\parallel} gives rise to a macroscopic in-plane polarization of real spins, whereas the real-spin polarization induced by an electric field \mathcal{E}_{\parallel} is anti-parallel in the two valleys.

The fields \mathbf{B}_{\parallel} and \mathcal{E}_{\parallel} also couple to the in-plane pseudospin σ_{\parallel} . Term (6) of Table I induces an out-of-plane tilt of the spin orientation of individual states which, in the \mathbf{K}' valley, has opposite signs for \mathbf{B}_{\parallel} and \mathcal{E}_{\parallel} . Remarkably, on average this yields an in-plane polarization $\langle \sigma_{\parallel} \rangle$ which is nonetheless the same in each valley for fields \mathbf{B}_{\parallel} and \mathcal{E}_{\parallel} (Fig. 2). This result reflects the fact that the macroscopic pseudospin polarization $\langle \sigma_{\parallel} \rangle$ is neither even nor odd under time reversal.¹⁷ More precisely, in each valley the direction of $\langle \sigma_{\parallel} \rangle$ is well-defined only up to a gauge-dependent angular offset. Yet the *change* of $\langle \sigma_{\parallel} \rangle$ induced by a change in the in-plane orientation of the applied field *is* well-defined and it points clockwise in one valley and counterclockwise in the other valley (for both \mathbf{B}_{\parallel} and \mathcal{E}_{\parallel} and all terms in Tab. I giving rise to an in-plane pseudospin orientation of individual states). Specifically for the term (6), if we change the in-plane orientation of the fields \mathbf{B}_{\parallel} or \mathcal{E}_{\parallel} by an angle φ , this changes the resulting average polarization $\langle \sigma_{\parallel} \rangle$ by $\pm 2\varphi$. This implies, in particular, that reverting the direction of the external field yields the same orientation of the induced pseudospin polarization. We see here that the pseudospin polarization induced by external fields \mathcal{E} and \mathbf{B} behaves qualitatively different from the polarization of real spins.

Numeric values for the prefactors of the field-dependent interactions in Fig. 2 cannot be determined with the methods used here, but the important qualitative trends do not depend on these values. Therefore, in the calculations yielding Fig. 2, the prefactors were chosen large enough to provide a visually clear picture.

B. Valley-contrasting axion electrodynamics

Up to now, we have considered implications of the magneto-electric equivalence for interactions that are linear in either \mathbf{B} or \mathcal{E} . In every material, we also have interactions proportional to the squared field components. In SLG, these are interactions proportional to B_{\parallel}^2 , B_z^2 , $\mathcal{E}_{\parallel}^2$ and \mathcal{E}_z^2 . The magneto-electric equivalence implies that we may replace one factor in the square of one field by the corresponding components of the other field. We thus get scalar magneto-electric couplings

$$c_{\parallel} \mathcal{E}_{\parallel} \cdot \mathbf{B}_{\parallel} \tau_z + c_z \mathcal{E}_z B_z \tau_z, \quad (3)$$

as well as their trigonally anisotropic counterpart

$$c_{\Delta} [(\mathcal{E}_y B_y - \mathcal{E}_x B_x) \sigma_x \tau_z + (\mathcal{E}_y B_x + \mathcal{E}_x B_y) \sigma_y \tau_0]. \quad (4)$$

Such scalars enter not only the Hamiltonian describing the dynamics of electrons in graphene, but they also enter the Lagrangian¹⁸ from which we obtain Maxwell's equations in graphene. The bi-linear coupling of electric and magnetic fields displayed in Eq. (3) is reminiscent of the $\mathcal{E} \cdot \mathbf{B}$ contribution to the Lagrangian of axions,⁸ hypothetical particles that were introduced to solve the strong CP problem in particle physics. Here the bi-linear couplings also have a valley dependence. Assuming independent dynamics for the electrons in the two valleys, the new term in the Lagrangian becomes

$$\mathcal{L}_{\text{ax}} = \sum_{\alpha=\mathbf{K},\mathbf{K}'} (-\nu_{\alpha}) (c_{\parallel} \mathcal{E}_{\parallel} \cdot \mathbf{B}_{\parallel} + c_z \mathcal{E}_z B_z), \quad (5)$$

where $\nu_{\mathbf{K}} = +1$ and $\nu_{\mathbf{K}'} = -1$. The presence of \mathcal{L}_{ax} modifies Gauss' law in BLG by inducing valley-dependent charge densities

$$\rho^{(\alpha)} = \nu_{\alpha} [\mathbf{B}_{\parallel} \cdot \nabla_{\parallel} c_{\parallel} + (c_{\parallel} - c_z) \nabla_{\parallel} \cdot \mathbf{B}_{\parallel}] \quad (6)$$

proportional to \mathbf{B}_{\parallel} , and it modifies Ampère's law by inducing current densities

$$\mathbf{j}_{\parallel}^{(\alpha)} = \nu_{\alpha} \hat{\mathbf{z}} \times [\mathcal{E}_z \nabla_{\parallel} c_z + (c_z - c_{\parallel}) \nabla_{\parallel} \mathcal{E}_z] \quad (7)$$

proportional to \mathcal{E}_z (see Appendix B for details), thus realizing a valley-contrasting axion electrodynamics in BLG, where the usual coupling¹⁸ of charges to electric fields (Gauss' law) and currents to magnetic fields (Ampère's law) is completely reversed.

The finiteness of any real sample leads to a spatial variation of the coefficients c_j at its edge. As a result, equilibrium valley-isospin *densities* are induced at the BLG sheet's boundaries in the xy plane when the magnetic field has an in-plane component directed perpendicularly to such a boundary; and a perpendicular electric field generates equilibrium valley-isospin *currents* flowing parallel to the system's boundaries in the xy plane. Figure 3 illustrates these effects in panels (a) and (b). The valley-asymmetric character of the edge densities and currents

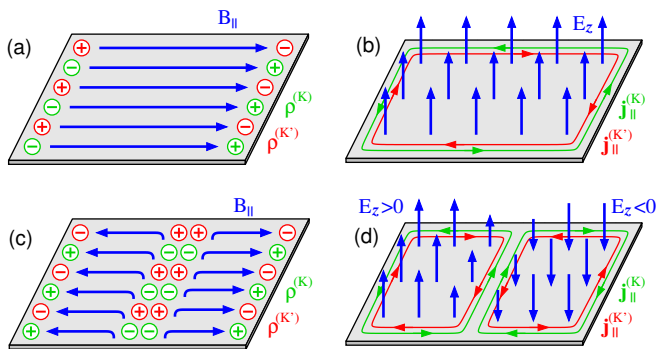


FIG. 3: Ramifications of the valley-contrasting axion electro-dynamics. (a) An in-plane magnetic field \mathbf{B}_{\parallel} induces equilibrium valley-isospin densities $\rho^{(\alpha)}$ at sample boundaries that are not aligned with \mathbf{B}_{\parallel} . (b) A perpendicular electric field \mathcal{E}_z gives rise to equilibrium valley-isospin edge currents $\mathbf{j}_{\parallel}^{(\alpha)}$. (c) Valley-isospin densities can be created inside the sample by engineering inhomogeneity in the in-plane magnetic field. (d) Valley-isospin currents can be created inside the sample by engineering inhomogeneity in the perpendicular electric field.

in BLG distinguishes them from similar edge effects in topological materials¹⁹ that generally require the presence of strong spin-orbit coupling. Also in contrast to the usually considered^{8,19} cases where $c_z = c_{\parallel}$, valley-isospin densities (currents) can be induced in the *bulk* of BLG by spatially inhomogeneous fields \mathbf{B}_{\parallel} (\mathcal{E}_z). Scenarios for this are illustrated in panels (c) and (d) of Fig. 3, which can be realized, e.g., by placing nanomagnets on the surface of a BLG sample [for (c)] or arranging pairs of front and back gates with opposite voltage polarity around adjacent parts of the sample²⁰ [for (d)]. More generally, the valley-contrasting axion electro-dynamics discovered here enlarges the scope of valley-dependent electronic effects in graphene materials^{21,22} by providing a comprehensive framework to design magneto-electric effects at boundaries and interfaces in BLG, including associated valley-helical edge states.^{20,23}

III. DISCUSSION AND OUTLOOK

One of the most exciting aspects of magneto-electric equivalence in BLG is the wide range of novel matter-field interactions resulting in this material. To achieve any type of effect within a valley, either an electric or a magnetic field component can be utilized. This includes, in particular, the different real-spin and pseudo-spin couplings of both Zeeman and spin-orbit character. Ingenious combinations of nano-magnetic and nano-electronic fabrication capabilities can thus be used to realize new device architectures that are impossible to achieve in other materials. Additional variability is provided by the valley-isospin degree of freedom, allowing the selective creation of global or valley-contrasting real-spin or pseudo-spin polarizations and their exploitation for both

fundamental research and new nano-spintronic applications. Finally, it is fascinating that the phenomena discussed here are present not only in bilayer graphene, but they exist in any material with similar symmetries. In particular, analogous behaviour can be realized in appropriately designed metamaterials^{24,25} or cold atoms in optical lattices.²⁶ The intrinsic tuneability of system parameters in these latter realizations opens intriguing avenues to tailor the relative magnitude of these matter-field interactions beyond the regime accessible in BLG.

Acknowledgments

The authors thank M. Meyer and H. Schultheiß for help with generating Fig. 2. Useful discussions with J. J. Heremans, A. H. MacDonald, J. L. Mañes, and M. Morgenstern are also gratefully acknowledged. This work was supported by Marsden Fund contract no. VUW0719, administered by the Royal Society of New Zealand, and at Argonne National Laboratory by the DOE BES via contract no. DE-AC02-06-CH11357.

Appendix A: Symmetry analysis and invariant expansion for BLG bandstructure: General discussion and results

The Hamiltonian (1) describes the band structure of graphene as a function of the wave vector \mathbf{k} measured from the \mathbf{K} point. The theory of invariants^{9,14} makes it possible to also include perturbations \mathcal{K} that are combinations of various quantities in addition to the wave vector \mathbf{k} , e.g., electric and magnetic fields \mathcal{E} and \mathbf{B} , strain ϵ and the intrinsic spin \mathbf{s} . The electron states at the \mathbf{K} point transform according to the two-dimensional irreducible representation (IR) Γ_3 of the group D_3 (Ref.27). The effective 2×2 Hamiltonian for the Γ_3 subspace can be expressed as

$$\mathcal{H}_{\mathbf{K}}(\mathcal{K}) = \sum_{\kappa, \lambda} a_{\kappa\lambda} \sum_{l=1}^{L_{\kappa}} X_l^{(\kappa)} \mathcal{K}_l^{(\kappa, \lambda)*}. \quad (\text{A1})$$

Here $a_{\kappa\lambda}$ are prefactors, $X_l^{(\kappa)}$ are 2×2 matrices that transform according to the IRs Γ_{κ} (of dimension L_{κ}) contained in the product representation $\Gamma_3 \times \Gamma_3^* = \Gamma_1 + \Gamma_2 + \Gamma_3$ of D_3 . Likewise, \mathcal{K} can be decomposed into irreducible tensor operators $\mathcal{K}^{(\kappa', \lambda)}$ that transform according to the IRs $\Gamma_{\kappa'}$ of D_3 . Using the coordinate system in Fig. 1 we obtain the basis matrices and tensor operators listed in Tables II and III.

Additional constraints for the Hamiltonian (A1) are due to time reversal invariance. The point group D_{3d} of BLG contains symmetry elements R mapping the basis functions $\Psi_{\mathbf{K}\lambda}$ at \mathbf{K} on $\Psi_{\mathbf{K}'\lambda}$ at \mathbf{K}' . These basis functions are also mapped onto each other by the time-reversal

operation θ , i.e., we have

$$\theta \Psi_{\mathbf{K},\lambda} = \Psi_{\mathbf{K}\lambda}^* = \sum_{\lambda'} \mathcal{T}_{\lambda\lambda'} \Psi_{\mathbf{K}'\lambda'}, \quad (\text{A2})$$

with a unitary matrix \mathcal{T} . Combining these operations, we obtain^{9,14,28}

$$\mathcal{T}^{-1} \mathcal{H}_{\mathbf{K}}(R^{-1}\mathcal{K})\mathcal{T} = \mathcal{H}_{\mathbf{K}}^*(\zeta\mathcal{K}) = \mathcal{H}_{\mathbf{K}}^t(\zeta\mathcal{K}). \quad (\text{A3})$$

Here t denotes transposition and ζ depends on the behavior of \mathcal{K} under time reversal. \mathbf{k} , \mathbf{B} , and \mathbf{s} are odd under time reversal so that then $\zeta = -1$, while \mathcal{E} and ϵ have $\zeta = +1$. Equation (A3) provides a general criterion for determining which terms in the expansion (A1) are allowed by time-reversal invariance and which terms are forbidden. The matrix \mathcal{T} depends on the choice for the operation R . If R is the reflection R_y at the yz plane [thus mapping the atoms in each sublattice in each layer onto each other, see Fig. 1(a)], we obtain

$$\mathcal{H}_{\mathbf{K}'}(\mathcal{K}) = \mathcal{H}_{\mathbf{K}}(R_y^{-1}\mathcal{K}) \quad . \quad (\text{A4})$$

and the matrix \mathcal{T} is simply the identity matrix.

We note that under R_y polar (\mathbf{p}) and axial (\mathbf{a}) vectors transform as

$$p_x \rightarrow -p_x \quad p_{y,z} \rightarrow p_{y,z} \quad , \quad (\text{A5a})$$

$$a_x \rightarrow a_x \quad a_{y,z} \rightarrow -a_{y,z} \quad . \quad (\text{A5b})$$

The transformational properties for the components of the second-rank strain tensor ϵ_{ij} can be expressed similarly.¹⁴ If we denote by τ_0 (τ_z) the unity (diagonal Pauli) matrix acting in valley-isospin space, Eq. (A5) can be summarized by writing general vector operators as $(p_x \tau_z, p_y \tau_0, p_z \tau_0)$ and $(a_x \tau_0, a_y \tau_z, a_z \tau_z)$.

The group D_3 characterizing the \mathbf{K} point in BLG is a subgroup of the group D_{3h} for the \mathbf{K} point in SLG²⁷ so that any term allowed by spatial symmetries in $\mathcal{H}_{\mathbf{K}}(\mathcal{K})$ for SLG is likewise allowed in BLG. Moreover, the constraint (A3) due to time reversal invariance is exactly equivalent to the constraint in SLG.⁹ Thus it follows immediately that the invariant expansion for BLG contains all terms that exist already for SLG.

A more detailed analysis shows that the point group D_{3h} for SLG distinguishes, as is usual, between polar vectors (such as the electric field \mathcal{E}) and axial vectors (such

TABLE II: Symmetrized matrices for the invariant expansion of the block \mathcal{H}_{33} for the point group D_3 .

Block	Representations	Symmetrized matrices
\mathcal{H}_{11}	$\Gamma_1 \times \Gamma_1^* = \Gamma_1$	$\Gamma_1 : (1)$
\mathcal{H}_{22}	$\Gamma_2 \times \Gamma_2^* = \Gamma_1$	$\Gamma_1 : (1)$
\mathcal{H}_{13}	$\Gamma_1 \times \Gamma_3^* = \Gamma_3$	$\Gamma_3 : (1, 1), (-i, i)$
\mathcal{H}_{23}	$\Gamma_2 \times \Gamma_3^* = \Gamma_3$	$\Gamma_3 : (1, -1), (-i, -i)$
\mathcal{H}_{33}	$\Gamma_3 \times \Gamma_3^*$	$\Gamma_1 : \mathbb{1}$
	$= \Gamma_1 + \Gamma_2 + \Gamma_3$	$\Gamma_2 : \sigma_z$
		$\Gamma_3 : \sigma_x, \sigma_y$

as the magnetic field \mathbf{B}). Thus each term in the SLG Hamiltonian with a certain functional form and linear in the field \mathcal{E} or \mathbf{B} is forbidden for the other field. However, the point group $D_3 \subset D_{3h}$ relevant for BLG contains only rotations as symmetry elements so that it cannot distinguish between polar and axial vectors. Therefore, the x and y components of any vector transform according to the IR Γ_3 , whereas the z component transforms according to Γ_2 . This implies that spatial symmetries cannot distinguish electric and magnetic fields in BLG. Moreover, Eq. (A3) treats electric and magnetic fields symmetrically, too. Thus it follows that every \mathcal{E} -dependent term

TABLE III: Irreducible tensor components for the point group D_3 (the group of the \mathbf{K} point in BLG). Terms printed in bold give rise to invariants in $\mathcal{H}_{\mathbf{K}}(\mathcal{K})$ allowed by time-reversal invariance. (No terms proportional to k_z are listed as they are irrelevant for graphene.) Contributions that are new in BLG (i.e., terms not allowed for the group D_{3h} of the \mathbf{K} point in SLG)⁹ are shown in red. Notation: $\{A, B\} \equiv \frac{1}{2}(AB + BA)$.

Γ_1	$1; \mathbf{k}_x^2 + \mathbf{k}_y^2; \{\mathbf{k}_x, 3\mathbf{k}_y^2 - \mathbf{k}_x^2\}; B_x k_x + B_y k_y; k_x \mathcal{E}_x + k_y \mathcal{E}_y; \mathcal{E}_x B_x + \mathcal{E}_y B_y; \mathcal{E}_z B_z; \epsilon_{xx} + \epsilon_{yy}; \epsilon_{zz}; (\epsilon_{yy} - \epsilon_{xx})\mathbf{k}_x + 2\epsilon_{xy}\mathbf{k}_y; \epsilon_{yz}\mathbf{k}_x - \epsilon_{xz}\mathbf{k}_y; (\epsilon_{yy} - \epsilon_{xx})B_x + 2\epsilon_{xy}B_y; \epsilon_{yz}B_x - \epsilon_{xz}B_y; (\epsilon_{yy} - \epsilon_{xx})\mathcal{E}_x + 2\epsilon_{xy}\mathcal{E}_y; \epsilon_{yz}\mathcal{E}_x - \epsilon_{xz}\mathcal{E}_y; s_x k_x + s_y k_y; s_x B_x + s_y B_y; s_z B_z; s_x \mathcal{E}_x + s_y \mathcal{E}_y; s_z \mathcal{E}_z; (s_x k_y - s_y k_x)\mathcal{E}_z; s_z (k_x \mathcal{E}_y - k_y \mathcal{E}_x); s_x(\epsilon_{yy} - \epsilon_{xx}) + 2s_y \epsilon_{xy}; s_x \epsilon_{yz} - s_y \epsilon_{xz}$
Γ_2	$\{k_y, 3k_x^2 - k_y^2\}; B_z; \mathbf{k}_x B_y - \mathbf{k}_y B_x; \mathcal{E}_z; \mathbf{k}_x \mathcal{E}_y - \mathbf{k}_y \mathcal{E}_x; \mathcal{E}_x B_y - \mathcal{E}_y B_x; (\epsilon_{xx} - \epsilon_{yy})k_y + 2\epsilon_{xy}k_x; \epsilon_{yz}k_y + \epsilon_{xz}k_x; (\epsilon_{xx} - \epsilon_{yy})B_y + 2\epsilon_{xy}B_x; (\epsilon_{xx} + \epsilon_{yy})B_z; \epsilon_{zz}B_z; \epsilon_{xz}B_x + \epsilon_{yz}B_y; (\epsilon_{xx} - \epsilon_{yy})\mathcal{E}_y + 2\epsilon_{xy}\mathcal{E}_x; (\epsilon_{xx} + \epsilon_{yy})\mathcal{E}_z; \epsilon_{zz}\mathcal{E}_z; \epsilon_{xz}\mathcal{E}_x + \epsilon_{yz}\mathcal{E}_y; s_z; s_x k_y - s_y k_x; s_x B_y - s_y B_x; s_x \mathcal{E}_y - s_y \mathcal{E}_x; (s_x k_x + s_y k_y)\mathcal{E}_z; s_y(\epsilon_{xx} - \epsilon_{yy}) + 2s_x \epsilon_{xy}; s_z(\epsilon_{xx} + \epsilon_{yy}); s_x \epsilon_{xz} + s_y \epsilon_{yz}; s_z \epsilon_{zz};$
Γ_3	$\mathbf{k}_x, \mathbf{k}_y; \{\mathbf{k}_y + \mathbf{k}_x, \mathbf{k}_y - \mathbf{k}_x\}; 2\{\mathbf{k}_x, \mathbf{k}_y\}; \{\mathbf{k}_x, \mathbf{k}_x^2 + \mathbf{k}_y^2\}, \{\mathbf{k}_y, \mathbf{k}_x^2 + \mathbf{k}_y^2\}; B_x, B_y; B_y k_y - B_x k_x; B_x k_y + B_y k_x; B_z k_y, -B_z k_x; \mathcal{E}_x, \mathcal{E}_y; \mathcal{E}_y k_y - \mathcal{E}_x k_x, \mathcal{E}_x k_y + \mathcal{E}_y k_x; \mathcal{E}_z k_y, -\mathcal{E}_z k_x; \mathcal{E}_y B_y - \mathcal{E}_x B_x, \mathcal{E}_y B_x + \mathcal{E}_x B_y; \mathcal{E}_y B_z, -\mathcal{E}_x B_z; \mathcal{E}_z B_y, -\mathcal{E}_z B_x; \epsilon_{yy} - \epsilon_{xx}, 2\epsilon_{xy}; \epsilon_{yz}, -\epsilon_{xz}; (\epsilon_{xx} + \epsilon_{yy})(\mathbf{k}_x, \mathbf{k}_y); \epsilon_{yz}k_x + \epsilon_{xz}k_y, \epsilon_{xz}k_x - \epsilon_{yz}k_y; (\epsilon_{xx} - \epsilon_{yy})\mathbf{k}_x + 2\epsilon_{xy}\mathbf{k}_y, (\epsilon_{yy} - \epsilon_{xx})\mathbf{k}_y + 2\epsilon_{xy}\mathbf{k}_x; \epsilon_{zz}k_x, \epsilon_{zz}k_y; (\epsilon_{xx} + \epsilon_{yy})(B_x, B_y); \epsilon_{yz}B_x + \epsilon_{xz}B_y, \epsilon_{xz}B_x - \epsilon_{yz}B_y; (\epsilon_{xx} - \epsilon_{yy})B_x + 2\epsilon_{xy}B_y, (\epsilon_{yy} - \epsilon_{xx})B_y + 2\epsilon_{xy}B_x; 2\epsilon_{xy}B_z, (\epsilon_{xx} - \epsilon_{yy})B_z; \epsilon_{zz}B_x, \epsilon_{zz}B_y; \epsilon_{xz}B_z, \epsilon_{yz}B_z; (\epsilon_{xx} + \epsilon_{yy})(\mathcal{E}_x, \mathcal{E}_y); \epsilon_{yz}\mathcal{E}_x + \epsilon_{xz}\mathcal{E}_y, \epsilon_{xz}\mathcal{E}_x - \epsilon_{yz}\mathcal{E}_y; (\epsilon_{xx} - \epsilon_{yy})\mathcal{E}_x + 2\epsilon_{xy}\mathcal{E}_y, (\epsilon_{yy} - \epsilon_{xx})\mathcal{E}_y + 2\epsilon_{xy}\mathcal{E}_x; 2\epsilon_{xy}\mathcal{E}_z, (\epsilon_{xx} - \epsilon_{yy})\mathcal{E}_z; \epsilon_{zz}\mathcal{E}_x, \epsilon_{zz}\mathcal{E}_y; \epsilon_{xz}\mathcal{E}_z, \epsilon_{yz}\mathcal{E}_z; s_x, s_y; s_y k_y - s_x k_x, s_x k_y + s_y k_x; s_z k_y, -s_z k_x; s_y B_y - s_x B_x, s_x B_y + s_y B_x; s_z B_y, -s_z B_x; s_y B_z, -s_x B_z; s_y \mathcal{E}_y - s_x \mathcal{E}_x, s_x \mathcal{E}_y + s_y \mathcal{E}_x; s_z \mathcal{E}_y, -s_z \mathcal{E}_x; s_y \mathcal{E}_z, -s_x \mathcal{E}_z; s_z (k_x \mathcal{E}_y + k_y \mathcal{E}_x), s_z (k_x \mathcal{E}_x - k_y \mathcal{E}_y); (s_x k_y + s_y k_x)\mathcal{E}_z, (s_x k_x - s_y k_y)\mathcal{E}_y; (s_x, s_y)(\epsilon_{xx} + \epsilon_{yy}); 2s_z \epsilon_{xy}, s_z(\epsilon_{xx} - \epsilon_{yy}); s_x(\epsilon_{xx} - \epsilon_{yy}) - 2s_y \epsilon_{xy}, s_y(\epsilon_{yy} - \epsilon_{xx}) - 2s_x \epsilon_{xy}; s_x \epsilon_{zz}, s_y \epsilon_{zz}; s_z \epsilon_{xz}, s_z \epsilon_{yz}; s_x \epsilon_{yz} + s_y \epsilon_{xz}, s_x \epsilon_{xz} - s_y \epsilon_{yz};$

in the BLG Hamiltonian (A1) is accompanied by another term where \mathcal{E} is simply replaced by \mathbf{B} (and vice versa for \mathbf{B} -dependent terms). However, the prefactors of these terms are, in general, unrelated.¹⁴ Table I summarizes some of the new terms arising from this magneto-electric equivalence.

Similar to SLG, pseudospin up and down in BLG corresponds to atoms in sublattice B and B' , see Fig. 1(a).²⁹ With the convention that for both valleys $v = \mathbf{K}, \mathbf{K}'$ the up and down eigenstates of pseudospin σ_z correspond to the same sublattice, the above procedure determines the Hamiltonians \mathcal{H}_v up to phases ϕ_v corresponding to pseudospin rotations $\tilde{\sigma}_j = \exp(i\phi_v\sigma_z/2)\sigma_j\exp(-i\phi_v\sigma_z/2)$ of the basis matrices σ_j ($j = x, y$) entering the invariant expansion (A1) (Ref.30). Due to this $U(1)$ gauge freedom the direction of the average in-plane spin polarization $\langle\boldsymbol{\sigma}_{\parallel}\rangle_v$ induced within a valley by fields \mathbf{B} and \mathcal{E} is well-defined only up to a uniform field-independent angular offset ϕ_v .

Appendix B: Valley-contrasting axion electrodynamics in BLG: Calculation of induced densities and currents

The presence of \mathcal{L}_{ax} leads to modifications of the inhomogeneous Maxwell's equations (i.e., Gauss' and Ampère's laws) amounting to the replacements⁸

$$\mathbf{D} \rightarrow \mathbf{D} - \sum_{\alpha} \nu_{\alpha} (c_{\parallel} \mathbf{B}_{\parallel} + c_z B_z \hat{\mathbf{z}}) \quad , \quad (\text{B1a})$$

$$\mathbf{H} \rightarrow \mathbf{H} + \sum_{\alpha} \nu_{\alpha} (c_{\parallel} \mathcal{E}_{\parallel} + c_z \mathcal{E}_z \hat{\mathbf{z}}) \quad , \quad (\text{B1b})$$

where \mathbf{D} and \mathbf{H} denote the macroscopic electric and magnetic fields in matter.¹⁸ Equations (B1) imply the existence of extra valley-dependent charge densities and currents that are most generally given by

$$\rho^{(\alpha)} = \nu_{\alpha} \boldsymbol{\nabla} \cdot (c_{\parallel} \mathbf{B}_{\parallel} + c_z B_z \hat{\mathbf{z}}) \quad , \quad (\text{B2a})$$

$$\mathbf{j}^{(\alpha)} = -\nu_{\alpha} \boldsymbol{\nabla} \times (c_{\parallel} \mathcal{E}_{\parallel} + c_z \mathcal{E}_z \hat{\mathbf{z}}) - \nu_{\alpha} \partial_t (c_{\parallel} \mathbf{B}_{\parallel} + c_z B_z \hat{\mathbf{z}}) \quad . \quad (\text{B2b})$$

The coefficients c_j are finite constants within BLG but must vanish outside the sample. Hence, there is a boundary contribution to $\boldsymbol{\nabla}c_j \equiv \boldsymbol{\nabla}_{\parallel}c_j$, and we have

$$\rho^{(\alpha)} = \nu_{\alpha} [(\boldsymbol{\nabla}_{\parallel}c_{\parallel}) \cdot \mathbf{B}_{\parallel} + c_{\parallel} \boldsymbol{\nabla} \cdot \mathbf{B}_{\parallel} + c_z \partial_z B_z] \quad . \quad (\text{B3})$$

Using the homogeneous Maxwell equation $\boldsymbol{\nabla} \cdot \mathbf{B} = 0$, the magnetic-field-induced charge densities are then given by

Eq. (6). Furthermore, the two-dimensionality of BLG implies that currents flow only in-plane. Hence, both $(\boldsymbol{\nabla}_{\parallel}c_{\parallel}) \times \mathcal{E}_{\parallel}$ and $\partial_t B_z \hat{\mathbf{z}}$ do not contribute to the current, which is just given by

$$\mathbf{j}^{(\alpha)} = -\nu_{\alpha} [c_{\parallel} (\boldsymbol{\nabla} \times \mathcal{E}_{\parallel} + \partial_t \mathbf{B}_{\parallel}) + \boldsymbol{\nabla} \times (c_z \mathcal{E}_z \hat{\mathbf{z}})] \quad . \quad (\text{B4})$$

The other homogeneous Maxwell equation can be written as $\boldsymbol{\nabla} \times \mathcal{E}_{\parallel} + \partial_t \mathbf{B}_{\parallel} = -\boldsymbol{\nabla} \times (\mathcal{E}_z \hat{\mathbf{z}}) - \partial_t B_z \hat{\mathbf{z}}$ whose in-plane projection inserted into Eq. (B4) yields Eq. (7). For homogeneous, time-independent fields \mathcal{E} and \mathbf{B} the ordinary couplings of \mathcal{E} and \mathbf{B} to ρ and \mathbf{j} vanish so that we only get the valley-contrasting axion electrodynamics of Eqs. (6) and (7).

The valley-contrasting axion electrodynamics discussed here can be expected to apply in situations when the valley-isospin degree of freedom is conserved. This will generally be the case for inhomogeneities induced by smoothly varying external fields (such as the one proposed in Ref.20). In contrast, the physical termination of the BLG sheet is abrupt on an atomic scale, and details will usually matter.³¹ Nevertheless, the recently observed²³ emergence of a universal behavior at disordered BLG edges consistent with that obtained from our valley-contrasting axion-electrodynamics suggests a wider applicability of this formalism.

Appendix C: Magnitude of Prefactors in Eq. (2)

Recent experiments³² demonstrated that a displacement field of ~ 1 V/nm generates a bandgap of ~ 0.1 eV in BLG, implying that $\lambda_z \sim 0.1$ e nm (with electron charge e) consistent with first-principles calculations.³³ For the remaining prefactors in Eq. (2), the Slonczewski-Weiss-McClure (SWM) model²⁹ applied to BLG yields (see also Ref.11)

$$g = \frac{4\gamma_0\gamma_4}{\gamma_1\gamma_a} \approx 6.2 \quad , \quad (\text{C1})$$

$$c_z = \frac{\gamma_0^2 + \gamma_4^2}{\gamma_1^2} \frac{\mu_B \lambda_z}{2\gamma_a} \approx 3 \times 10^{-4} \text{ e nm/T} \quad . \quad (\text{C2})$$

The SWM parameters γ_0 , γ_1 , and γ_4 are defined in Ref.29, and we have $\gamma_a = 2\hbar^2/(3m_0a^2)$, where m_0 is the electron mass in vacuum and a is the lattice constant of BLG's planar honeycomb structure.

¹ U. Rössler, *Solid State Theory - An Introduction* (Springer, Heidelberg, 2009), 2nd ed.

² A. K. Geim and K. S. Novoselov, *Nature Mater.* **6**, 183

(2007).

³ A. H. Castro Neto, F. Guinea, N. M. R. Peres, K. S. Novoselov, and A. K. Geim, *Rev. Mod. Phys.* **81**, 109

- (2009).
- ⁴ J. Moore, Nature Phys. **5**, 378 (2009).
 - ⁵ K. S. Novoselov, E. McCann, S. V. Morozov, V. I. Fal'ko, M. I. Katsnelson, U. Zeitler, D. Jiang, F. Schedin, and A. K. Geim, Nature Phys. **2**, 177 (2006).
 - ⁶ E. McCann and V. I. Fal'ko, Phys. Rev. Lett. **96**, 086805 (2006).
 - ⁷ A. K. Geim, Science **324**, 1530 (2009).
 - ⁸ F. Wilczek, Phys. Rev. Lett. **58**, 1799 (1987).
 - ⁹ R. Winkler and U. Zülicke, Phys. Rev. B **82**, 245313 (2010).
 - ¹⁰ T. Ohta, A. Bostwick, T. Seyller, K. Horn, and E. Rotenberg, Science **313**, 951 (2006).
 - ¹¹ L. M. Zhang, M. M. Fogler, and D. P. Arovas, Phys. Rev. B **84**, 075451 (2011).
 - ¹² M. Nakamura, E. V. Castro, and B. Dóra, Phys. Rev. Lett. **103**, 266804 (2009).
 - ¹³ M. Koshino and E. McCann, Phys. Rev. B **81**, 115315 (2010).
 - ¹⁴ G. L. Bir and G. E. Pikus, *Symmetry and Strain-Induced Effects in Semiconductors* (Wiley, New York, 1974).
 - ¹⁵ R. Winkler, *Spin-Orbit Coupling Effects in Two-Dimensional Electron and Hole Systems* (Springer, Berlin, 2003).
 - ¹⁶ C. L. Kane and E. J. Mele, Phys. Rev. Lett. **95**, 226801 (2005).
 - ¹⁷ R. Winkler and U. Zülicke, Phys. Lett. A **374**, 4003 (2010).
 - ¹⁸ J. D. Jackson, *Classical Electrodynamics* (Wiley, New York, 1999), 3rd ed.
 - ¹⁹ X.-L. Qi, T. L. Hughes, and S.-C. Zhang, Phys. Rev. B **78**, 195424 (2008).
 - ²⁰ I. Martin, Y. M. Blanter, and A. F. Morpurgo, Phys. Rev. Lett. **100**, 036804 (2008).
 - ²¹ D. Xiao, W. Yao, and Q. Niu, Phys. Rev. Lett. **99**, 236809 (2007).
 - ²² A. Rycerz, J. Tworzydło, and C. W. J. Beenakker, Nature Phys. **3**, 172 (2007).
 - ²³ J. Li, I. Martin, M. Büttiker, and A. F. Morpurgo, Nature Phys. **7**, 38 (2011).
 - ²⁴ M. Gibertini, A. Singha, V. Pellegrini, M. Polini, G. Vignale, A. Pinczuk, L. N. Pfeiffer, and K. W. West, Phys. Rev. B **79**, 241406 (2009).
 - ²⁵ K. K. Gomes, W. Mar, W. Ko, F. Guinea, and H. C. Manoharan, Nature **483**, 306 (2012).
 - ²⁶ L. Tarruell, D. Greif, T. Uehlinger, G. Jotzu, and T. Esslinger, Nature **483**, 302 (2012).
 - ²⁷ G. F. Koster, J. O. Dimmock, R. G. Wheeler, and H. Statz, *Properties of the Thirty-Two Point Groups* (MIT, Cambridge, MA, 1963).
 - ²⁸ J. L. Mañes, F. Guinea, and M. A. H. Vozmediano, Phys. Rev. B **75**, 155424 (2007).
 - ²⁹ J. W. McClure, Phys. Rev. **108**, 612 (1957).
 - ³⁰ L. C. Lew Yan Voon and M. Willatzen, *The $k \cdot p$ Method* (Springer, Berlin, 2009).
 - ³¹ J. Li, A. F. Morpurgo, M. Büttiker, and I. Martin, Phys. Rev. B **82**, 245404 (2010).
 - ³² Y. Zhang, T.-T. Tang, C. Girit, Z. Hao, M. C. Martin, A. Zettl, M. F. Crommie, Y. R. Shen, and F. Wang, Nature **459**, 820 (2009).
 - ³³ S. Konschuh, M. Gmitra, D. Kochan, and J. Fabian, Phys. Rev. B **85**, 115423 (2012).